Author(s): Hu, F. M. & Wehling, T. O. & Gubernatis, J. E. & Frauenheim, Thomas & Nieminen, Risto M.

Title: Magnetic impurity affected by spin-orbit coupling: Behavior near a topological phase transition

Year: 2013

Version: Final published version

Please cite the original version:

Hu, F. M. & Wehling, T. O. & Gubernatis, J. E. & Frauenheim, Thomas & Nieminen, Risto M. 2013. Magnetic impurity affected by spin-orbit coupling: Behavior near a topological phase transition. Physical Review B. Volume 88, Issue 4. 045106/1-6. 1550-235X (electronic). DOI: 10.1103/physrevb.88.045106.

Magnetic impurity affected by spin-orbit coupling: Behavior near a topological phase transition

F. M. Hu,[1] T. O. Wehling,[2,3] J. E. Gubernatis,[4] Thomas Frauenheim,[3] and R. M. Nieminen[1]

[1]*COMP/Department of Applied Physics, Aalto University School of Science, P.O. Box 11100, FI-00076 Aalto, Espoo, Finland*

[2]*Institute of Theoretical Physics, University of Bremen, Otto-Hahn-Allee 1, D-28359 Bremen, Germany*

[3]*Bremen Center for Computational Materials Science, University of Bremen, Am Fallturm 1a, D-28359 Bremen, Germany*

[4]*Theoretical Division, Los Alamos National Laboratory, Los Alamos, New Mexico 87545, USA*

(Received 29 January 2013; revised manuscript received 13 May 2013; published 3 July 2013)

We investigate the effect of spin-orbit coupling on the behavior of a magnetic impurity at the edge of a zigzag graphene ribbon by means of quantum Monte Carlo simulations. A peculiar interplay of Kane-Mele type spin-orbit and impurity-host coupling is found to greatly affect properties for the local moment. The local characters of the impurity are mainly dominated by the local density of states at the edge, such as double occupancy, magnetic moment, and spin susceptibilities. The special helical nature of the topological insulator on the boundary is found to affect nonlocal quantities, such as the two-particle and spin-spin correlation functions linking electrons on the impurity with those in the conduction band; in particular, due to the spin-orbit coupling, the symmetry of the spin rotation in the Kondo cloud around the impurity is partly broken.

DOI: 10.1103/PhysRevB.88.045106 PACS number(s): 73.22.Pr, 71.55.Jv, 75.30.Hx

I. INTRODUCTION

Spin-orbit coupling (SOC) plays a central role in topological insulator (TI) materials;[1] it opens a gap inside the bulk but supports the gapless electron states on the boundary. On the boundary of a TI, impurity potential scattering is restricted by time-reversal symmetry:[2,3] the backscattering among the electrons is allowed only if it is accompanied by a spin flip. This restriction gives rise to novel Kondo physics of magnetic impurities in a TI.[4,5] Accordingly, the behavior of magnetic impurities in host materials with SOC has recently attracted interest. In two-dimensional (2D) systems, several theoretical papers[6,7] report that the presence of the SOC can, in general, protect the impurity's magnetic moment from being totally screened. However, for the specific case of the Rashba coupling[8,9] it has been reported that the SOC only makes a small or a high-order contribution to Kondo scaling.

In general, SOC and energies associated with the Kondo screening of magnetic impurities can be of the same order of magnitude. It remains to be explored what effects arise when crossing over from weak to strong SOC. In particular, the question of how the impurity behaves when the host undergoes a topological phase transition from a normal state to a TI is still an open question.

In this paper, we consider an Anderson impurity at the edge of a zigzag graphene ribbon[10] with a Kane-Mele type SOC gradually strengthened, so that a topological phase transition occurs in the system. Using quantum Monte Carlo (QMC) simulations at finite temperature, we perform a comprehensive study on the properties of the impurity. Calculating local physical quantities on the impurity site, such as the average double occupancy, magnetic moment, and spin susceptibility, we find that, in general, the SOC can support the local moment formation. We see that in the case of zero or weak SOC, the local properties of the impurity are mainly dominated by its coupling with localized edge states, realizing a situation similar to the zero bandwidth Anderson (ZBWA) model. In the case of strong SOC, the edge states are greatly broadened and thus the local density of states (LDOS) is suppressed, so that the impurity behaves as a spin in a normal metal. This difference between strong and weak coupling also manifests itself in the dependence of the local moment on the chemical potential, which in graphene can be tuned by a gate voltage. So the local characters of the impurity are governed by the LDOS at the edge. We also study the nonlocal linking of the electrons on the impurity with those in the conduction band. In nonlocal two-particle correlations, we observe a set of distinct spin-momentum relations which show the helical locking and interplay between backscattering and spin flip. This interplay signals the appearance of a topological phase in the host. Additionally, we find the spin rotation symmetry in the Kondo cloud around the impurity to be partially broken by the SOC. This finding agrees with a previous study of an Anderson impurity in a 2D helical metal with a variational method that is valid for a large Coulomb interaction.[6] In this work, we study the effect of the electron-electron interaction over a wide regime and document that the Coulomb interaction enhances the anisotropy in the spin-spin correlation function and plays a complicated role in spin and momenta scattering. So the topological phase transition is clearly reflected by the correlation functions of the impurity and conducting-band electrons.

II. MODEL AND METHODS

Our starting point is the Hamiltonian

$$H = H_{\text{K-M}} + H_1 + H_2, \tag{1}$$

where $H_{\text{K-M}}$ is the Kane-Mele model in a zigzag edge graphene ribbon.[11] It has two pieces: $H_{\text{K-M}} = H_t + H_{\text{so}}$, with H_t being the usual nearest-neighbor hopping of the tight-binding model in graphene,

$$H_t = -t \sum_{\langle ij\rangle,\sigma} (c^\dagger_{i,\sigma} c_{j,\sigma} + \text{H.c.}) - \mu \sum_{i,\sigma} c^\dagger_{i,\sigma} c_{i,\sigma},$$

here $c^\dagger_{i,\sigma}$ creates an electron with spin σ on the ith site in graphene, and t and μ are the hopping parameter and chemical potential in the system. And

$$H_{\text{so}} = \lambda \sum_{\langle\langle ij\rangle\rangle} (i\nu_{ij} c^\dagger_i \sigma^z c_j + \text{H.c.}).$$

H_{so} is the SOC term and σ^z is the z Pauli matrix. H_{so} thus has opposite signs for opposite electron spins. The parameters $v_{ij} = -v_{ji} = \pm 1$ depend on the orientation of the two nearest-neighbor bonds as the electron hops from site i to j: $v_{ij} = +1$ if the electron makes a left turn to the second bond. It is negative if it makes a right turn. H_1 is the impurity Hamiltonian

$$H_1 = \sum_\sigma (\varepsilon_d - \mu) d_\sigma^\dagger d_\sigma + U d_\uparrow^\dagger d_\uparrow d_\downarrow^\dagger d_\downarrow .$$

Here $d_\sigma^\dagger$ creates an electron with spin σ in the impurity orbit, and U is the Coulomb repulsion inhibiting the simultaneous occupancy of the orbital by two electrons. Finally H_2 describes the hybridization between the impurity and one of the atoms on the edge (located at the A-sublattice site R_{a0}),

$$H_2 = V \sum_\sigma [c_{a0,\sigma}^\dagger d_\sigma + d_\sigma^\dagger c_{a0,\sigma}] .$$

Our principal computational tools are the single-impurity QMC algorithm[12] for computing the local thermodynamic properties of the impurity. The QMC method naturally returns the imaginary-time Green's function $G_{d\sigma}(\tau > 0) = \langle d_\sigma(\tau) d_\sigma^\dagger \rangle$ of the impurity. With this Green's function, we can easily compute the magnetic quantities on the impurity site such as the expected values of the magnet moment squared $\langle (S^z)^2 \rangle = \langle (d_\uparrow^\dagger d_\uparrow - d_\downarrow^\dagger d_\downarrow)^2 \rangle$, the double occupancy $\langle n_{d\uparrow} n_{d\downarrow} \rangle = \langle d_\uparrow^\dagger d_\uparrow d_\downarrow^\dagger d_\downarrow \rangle$, and the static impurity spin susceptibility

$$\chi = \int_0^\beta d\tau \langle S^z(\tau) S^z(0) \rangle, \tag{2}$$

where $\beta = T^{-1}$, and $S^z(\tau) = e^{\tau H} S^z(0) e^{-\tau H}$. Using an extended QMC algorithm,[13] we can calculate Green's function linking electrons on the impurity site and those in the conduction bands: $G_{di\sigma}(\tau > 0) = \langle d_\sigma(\tau) c_{i\sigma}^\dagger \rangle$ or $G_{id\sigma}(\tau > 0) = \langle c_{i\sigma}(\tau) d_\sigma^\dagger \rangle$.

III. IN THE LARGE-U LIMIT: s-d EXCHANGE MODEL

Before we do the QMC simulation, to gain insight into this problem, we map the original Hamiltonian, Eq. (1), to the impurity's single-occupancy subspace in the large-U limit. Defining projection operators,[14]

$$\begin{aligned} P_0 &= (1 - n_{d\uparrow})(1 - n_{d\downarrow}), \\ P_1 &= n_{d\uparrow}(1 - n_{d\downarrow}) + n_{d\downarrow}(1 - n_{d\uparrow}), \\ P_2 &= n_{d\uparrow} n_{d\downarrow}, \end{aligned} \tag{3}$$

and we can solve the effective Hamiltonian in single-occupancy subspace as

$$\tilde{H} = H_{11} + H_{12}(E - H_{22})^{-1} H_{21} + H_{10}(E - H_{00})^{-1} H_{01} . \tag{4}$$

Here $H_{ij} = P_i H P_j$ and $H_{ij} = H_{ji}^\dagger$; then an effective s-d exchange model has the formula as

$$\begin{aligned} \tilde{H} = \frac{1}{N} \sum_{kk'll'} & [S^z (J^\perp_{kk'll'\uparrow} c_{kl\uparrow}^\dagger c_{k'l'\uparrow} - J^\perp_{kk'll'\downarrow} c_{kl\downarrow}^\dagger c_{k'l'\downarrow})] \\ & + [J^\parallel_{kk'll'} S^+ c_{kl\downarrow}^\dagger c_{k'l'\uparrow} + \text{H.c.}], \end{aligned}$$

$$\begin{aligned} J^\perp_{kk'll'\sigma} &= V^a_{kl\sigma} V^{a*}_{k'l'\sigma} \left[\frac{V^2}{U + \varepsilon_d - E_{k'l'}} + \frac{V^2}{E_{kl} - \varepsilon_d} \right], \\ J^\parallel_{kk'll'} &= V^a_{kl\downarrow} V^{a*}_{k'l'\uparrow} \left[\frac{V^2}{U + \varepsilon_d - E_{k'l'}} + \frac{V^2}{E_{kl} - \varepsilon_d} \right], \end{aligned} \tag{5}$$

in which $S^+ = d_\uparrow^\dagger d_\downarrow$, and $V^a_{kl\sigma}$ is the amplitude of the eigenstate at R_{a0} at the edge; here k and l are indexes of momentum and band, respectively. Furthermore, $V^a_{kl\sigma}$ relates the Fermi operators in real space to those in eigenspace,

$$c_{ar,\sigma}^\dagger = \frac{1}{\sqrt{N}} \sum_{kl} e^{-ikr} V^a_{kl\sigma} c_{kl\sigma}^\dagger, \tag{6}$$

where N is the number of atoms at the edge. Therefore we see that $\tilde{H}$ is different from the normal s-d exchange model because of the broken symmetry, $J^\perp_{kk'll'\sigma} \neq J^\parallel_{kk'll'}$, which is due to the helical properties driven by the SOC. Later we will see this asymmetry more clearly in the spin-flip scattering. If we consider that the impurity is mainly scattered by the levels near the Fermi level and $-\varepsilon_d = \frac{U}{2} \gg |\mu|$, there are $J^\perp_{kk'll'\sigma} \approx \frac{4V^2}{U} V^a_{kl\sigma} V^{a*}_{k'l'\sigma}$ and $J^\parallel_{kk'll'} \approx \frac{4V^2}{U} V^a_{kl\downarrow} V^{a*}_{k'l'\uparrow}$.

In Hamiltonian (5), the total amplitude of spin exchange depends on the sum $\sum_{kk'll'}$; in particular, the elastic exchange is determined by the sum $\sum_{kk'l}$, which is just the density of states (the degeneracy) on the level l. Figure 1(a) shows the LDOS at the edge, and we see that when $\lambda = 0$, a sharp peak exists at the Dirac point ($E/t = 0$) suggesting the existence of a strongly localized edge states. When $\lambda \neq 0$, the central peaks becomes smooth, and at $\lambda = 0.2t$, their values near $E/t = 0$ approach a constant and thus near the Dirac point become similar to the LDOS in a normal metal. First, we can expect that since the SOC decreases the LDOS at the edge, the spin exchange between impurity and conduction electrons will be suppressed.

Second, we focus our attention on a special process, elastic backscattering accompanied by a spin flip between a Kramers pair $(\pi \pm k, \sigma\bar{\sigma})$; in the following we denote this pair as $(k\sigma, -k\bar{\sigma})$. In this process, the transversal exchange $J^\parallel_{k-kl}$ is nonzero, but due to the helical phase at the edge, it has no corresponding vertical term in $\tilde{H}$, and $J^\perp_{k-kl\sigma} = 0$. Thus the symmetry in the s-d exchange model (5) is broken by the SOC. The weight of this spin-flip scattering, $S^+ c_{kl\downarrow}^\dagger c_{-kl\uparrow}$, depends on the coupling strength $J^\parallel_{k-kl}$, which is shown as the function of λ in Fig. 1(b). Here the momentum $k = 0.0025\pi$ and l is the first band under the zero point. We see that $J^\parallel_{k-kl}$ is totally equal to zero in the negative regime of λ but in the positive regime has finite value.

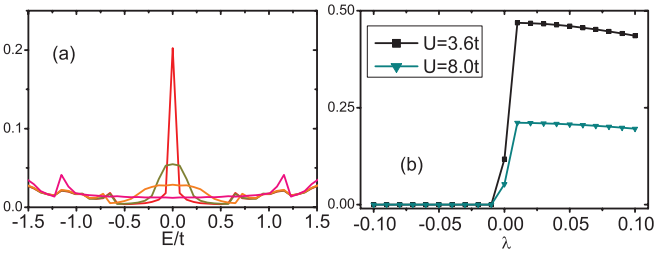

FIG. 1. (Color online) (a) The LDOS as a function of energy E/t with different values for λ. From top to bottom $\lambda = 0, 0.04t, 0.08t$, and $0.2t$. (b) The spin-flip strength $J^\parallel_{k-kl}$ as a function of λ.

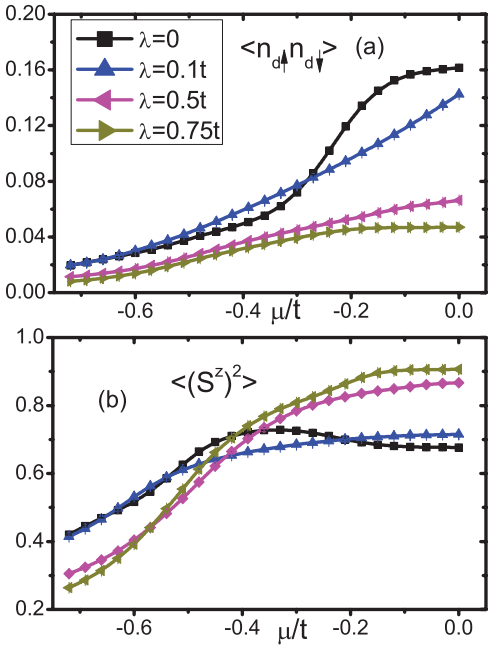

FIG. 2. (Color online) (a) Double occupancy $\langle n_{d\uparrow}n_{d\downarrow}\rangle$ versus chemical potential μ/t. (b) $\langle (S^z)^2\rangle$ versus μ/t. Here, $U = 1.2t$, $V = 0.65t$, $\varepsilon_d = -U/2$, and $T^{-1} = 32t^{-1}$.

This is due to helical properties at the edge: with positive SOC, the spin-up and spin-down electrons have momenta $-k$ and k, respectively, so both $V^a_{k\downarrow}$ and $V^{a*}_{-k\uparrow}$ have nonzero values but vanish when λ changes the sign and the electrons will move along opposite directions. Moreover, in Fig. 1(b) we see that the strength of spin flip $J^{\parallel}_{k-kl}$ decreases as the SOC increases in the large-U limit.

IV. NUMERICAL RESULTS

A. Local properties of the impurity

In this section, we will display our QMC results for both local and nonlocal properties for the impurity. To see the behavior of the local magnetic moment, in Fig. 2, we show double occupancy $\langle n_{d\uparrow}n_{d\downarrow}\rangle$ and local moment squared $\langle (S^z)^2\rangle$ versus the chemical potential μ/t which can be tuned by an electric field in graphene. With $\varepsilon_d = -U/2$ fixed and μ near the zero point, the impurity site is half filled, and thus the magnetic moment is driven by avoiding the possibility of double occupancy. In Fig. 2(b) we see that increasing the SOC results in the average double occupancy $\langle n_{d\uparrow}n_{d\downarrow}\rangle$ decreasing because the SOC suppresses the effective hybridization between impurity and edge states. Near the Dirac point, the average local magnetic moment $\langle (S^z)^2\rangle$ is enhanced by the SOC. We also note that with weak SOC, the maxima of $\langle (S^z)^2\rangle$ are not at $\mu = 0$, while for the large λ, they are at $\mu = 0$. We comment that with small SOC the localized states on the edge are antiferromagnetically coupled to impurity states below the Fermi energy, so shifting μ from zero can decouple these oppositely aligned spin states and lead to the development of a magnet moment.[15] Contrary to the weak SOC case, the strong SOC greatly broadens the central peak in LDOS on the edge, making the LDOS near the Fermi energy similar to that of a normal metal. Thus we see that half filling

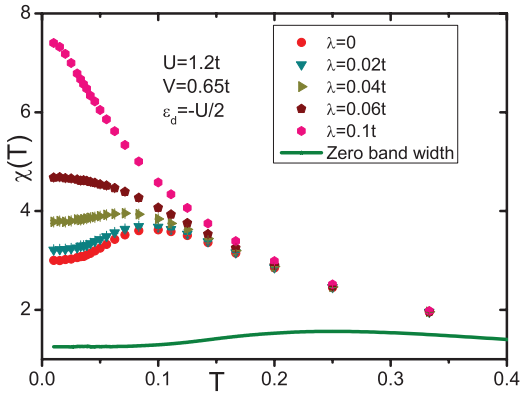

FIG. 3. (Color online) The spin susceptibility χ as a function of T for different values of the SOC. $U = 1.2t$, $V = 0.65t$, $\varepsilon_d = -U/2$, and $\mu = 0$. The solid line presents the results for the ZBWA model.

(hole-particle symmetry) optimizes the magnetic moment at $\mu = 0$.

In order to see the formation of local moment and screening around it, we study the dynamical behavior of spin susceptibility in Eq. (2); in Fig. 3 we show χ as a function of temperature for different values of λ. We fix the hole-particle symmetry by setting $\mu = 0$ and $\varepsilon_d = -U/2$. Doing so means the average electron occupancy of the impurity site is 1, i.e., it is half filled. From the figure, we also see that with small $0 < \lambda < 0.06t$ and the lowering of the temperature, the spin susceptibility first increases, then decreases, and finally saturates (totally screened). But when $0.06t < \lambda < 0.1t$, χ first increases and then directly becomes saturated. We note that when the SOC is gradually switched on, χ goes cross over from the behavior in the ZBWA model (solid line in Fig. 3) to that in a normal metal.[14] We propose this transition occurs because of the LDOS being decreased by the SOC, consequently, the spin exchange between the impurity and conduction electrons is suppressed.

From Figs. 2 to 3, we mainly show the local properties on the impurity site, which are exactly governed by the edge states modified by the SOC. The central resonant in LDOS is broadened by the SOC, and the region near the Dirac point approaches a constant. So as the SOC is increasing in the system, the impurity coupled to the edge states crosses over from a spin in a band with zero width to one in a normal metal. However, these local physical quantities cannot reflect the natures of quantum spin Hall states, and in the following part, we will display the nonlocal correlation between the impurity and conduction electrons, which directly characterizes the helical edge.

B. Nonlocal properties of impurity

The most interesting property of a TI boundary is the time-reversal invariance causing backscattering always being accompanied by spin-flip scattering. In Fig. 4, the spin-flip processes in the normal states and helical phase are shown. In the normal states, both forward and back spin-flip scatterings are allowed at the edge, while in the helical phase, on each edge, only one process exits for the right or left mover with a fixed spin orientation.

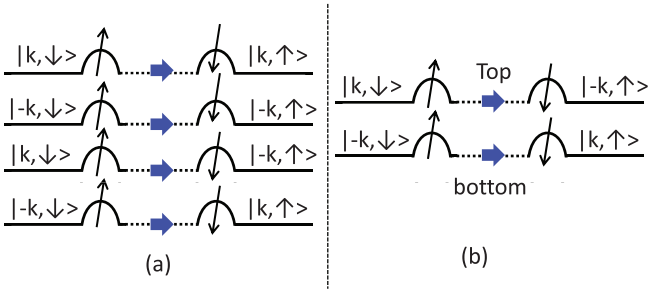

FIG. 4. (Color online) (a) The spin-flip processes in the normal states. (b) The spin-flip processes on the helical edges. $|\pm k, \uparrow\downarrow\rangle$ are the states of conduction electrons and up and down arrows mean local spins.

In order to directly see the signatures of spin-flip scattering, we computed a set P_k of two-particle correlation functions between the impurity and Kramers pair with momentum k: $P_k = \{\langle c_{k,\uparrow} d^\dagger_\uparrow d_\downarrow c^\dagger_{-k,\downarrow}\rangle, \langle c_{-k,\uparrow} d^\dagger_\uparrow d_\downarrow c^\dagger_{k,\downarrow}\rangle, \langle c_{k,\uparrow} d^\dagger_\uparrow d_\downarrow c^\dagger_{k,\downarrow}\rangle, \langle c_{-k,\uparrow} d^\dagger_\uparrow d_\downarrow c^\dagger_{-k,\downarrow}\rangle\}$. When $\lambda \neq 0$, due to the helical properties at the edge, with positive λ the correlation function $\langle c_{-k,\uparrow} d^\dagger_\uparrow d_\downarrow c^\dagger_{k,\downarrow}\rangle$ is nonzero but with negative λ it is always equal to zero. For $\langle c_{k,\uparrow} d^\dagger_\uparrow d_\downarrow c^\dagger_{-k,\downarrow}\rangle$, the situation is completely opposite. As for forward scattering with a spin flip, when the system is in the helical liquid phase, these processes are forbidden, namely, when $\lambda \neq 0$, the correlation functions $\langle c_{k,\uparrow} d^\dagger_\uparrow d_\downarrow c^\dagger_{k,\downarrow}\rangle = \langle c_{-k,\uparrow} d^\dagger_\uparrow d_\downarrow c^\dagger_{-k,\downarrow}\rangle = 0$. In our numerical results, we clearly see these characters.

In Fig. 5(a), we focus on one correlation function of P_k, $\langle c_{-k,\uparrow} d^\dagger_\uparrow d_\downarrow c^\dagger_{k,\downarrow}\rangle$ with momentum $k = 0.00125\pi$ in the first band below the Dirac point. We do the simulation varying λ and U, and we see that with the large Coulomb interaction $U = 5.4t$, in a wide regime, increasing the SOC slightly suppresses this correlation; this behavior agrees with that of transverse strength $J^\parallel$ in the s-d exchange Hamiltonian $\tilde{H}$ in Eq. (5) [shown in Fig. 1(b)] in the large-U limit. While with small and medium U, in the regime $0 < \lambda < 0.1t$, increasing the SOC enhances the spin-flip process. We attribute this point to the double occupancy decreased by the SOC; consequently, the local moment of impurity is developed. In Fig. 5(b), we show the results of $\langle n_{d\uparrow} n_{d\downarrow}\rangle$ as a function of λ with different values for U; in particular, at $U = 5.4t$, $\langle n_{d\uparrow} n_{d\downarrow}\rangle$ is close to zero. We comment that in the large-U limit, because the double occupancy is zero and the local moment has been well developed, the backscattering with a spin flip is mainly controlled by the properties for $V^{a0}_{kl\sigma}$ of the Kane-Mele Hamiltonian, while with small or medium Coulomb interaction, the double occupancy dominates.

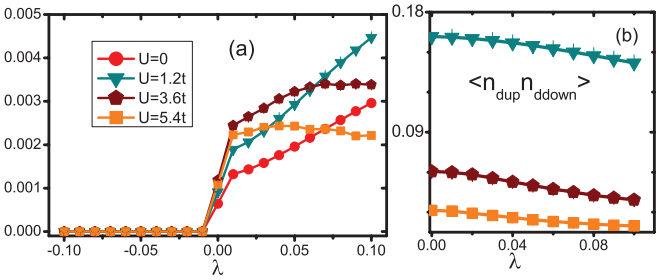

FIG. 5. (Color online) (a) Correlation function for backscattering and spin flip, $\langle c_{-k,\uparrow} d^\dagger_\uparrow d_\downarrow c^\dagger_{k,\downarrow}\rangle$ versus λ; (b) double occupancy as a function of λ. In both panels $V = 0.65t$, $\varepsilon_d = -U/2$, $\mu = 0$, $\beta = 32t^{-1}$, and momentum $k = 0.00125\pi$.

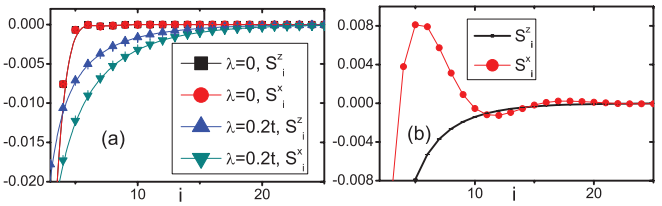

FIG. 6. (Color online) Spin-spin correlation functions $S^z_{\mathbf{i}}$ and $S^x_{\mathbf{i}}$ versus the index $\mathbf{i}$ at the edge, $U = 1.2t = -2\varepsilon_d$, and $\beta = 32t^{-1}$. In (a) $\mu = 0$ and in (b) $\mu = -0.2t$ and $\lambda = 0.15t$.

Using the same algorithm as those used for computing P_k, we computed the spatial distribution of the Kondo cloud described by spin-spin correlation functions $S^z_{\mathbf{i}}$, $S^x_{\mathbf{i}}$, and $S^y_{\mathbf{i}}$ defined as $S^z_{\mathbf{i}} = \langle (d^\dagger_\uparrow d_\uparrow - d^\dagger_\downarrow d_\downarrow)(c^\dagger_{\mathbf{i}\uparrow} c_{\mathbf{i}\uparrow} - c^\dagger_{\mathbf{i}\downarrow} c_{\mathbf{i}\downarrow})\rangle$, $S^x_{\mathbf{i}} = \langle (d^\dagger_\uparrow d_\downarrow + d^\dagger_\downarrow d_\uparrow)(c^\dagger_{\mathbf{i}\uparrow} c_{\mathbf{i}\downarrow} + c^\dagger_{\mathbf{i}\downarrow} c_{\mathbf{i}\uparrow})\rangle$, and $S^y_{\mathbf{i}} = (-i)^2 \langle (d^\dagger_\uparrow d_\downarrow - d^\dagger_\downarrow d_\uparrow)(c^\dagger_{\mathbf{i}\uparrow} c_{\mathbf{i}\downarrow} - c^\dagger_{\mathbf{i}\downarrow} c_{\mathbf{i}\uparrow})\rangle$, and $\mathbf{i}$ is the index of the A-sublattice at the edge. In these correlation functions, we find that the spin rotational symmetry is partly broken by the SOC, i.e., $S^z_{\mathbf{i}} \neq S^x_{\mathbf{i}}$ but $S^y_{\mathbf{i}} = S^x_{\mathbf{i}}$, and this asymmetry agrees with what was found for an impurity in the two-dimensional helical metal.[6] In Fig. 6(a), we show $S^{z(x)}_{\mathbf{i}}$ in the case of $\mu = 0$, and it is clear that at $\lambda = 0$, $S^z_{\mathbf{i}} = S^x_{\mathbf{i}}$ while when $\lambda \neq 0$, this symmetry is broken; furthermore at $\mu = 0$, both $S^z_{\mathbf{i}}$ and $S^x_{\mathbf{i}}$ have no oscillation behaviors. In Fig. 6(b), in the case of $\mu \neq 0$ and $\lambda \neq 0$, $S^z_{\mathbf{i}}$ still has no oscillation as

$$S^z_{\mathbf{i}} \propto \frac{-1}{f(R_{\mathbf{i}})},$$

but $S^x_{\mathbf{i}}$ has decaying as well as oscillation

$$S^x_{\mathbf{i}} \propto \frac{-1}{g(R_{\mathbf{i}})} \cos 2\phi R_{\mathbf{i}}.$$

$f(R_{\mathbf{i}})$ and $g(R_{\mathbf{i}})$ are two monotonically decreasing functions of distance from the impurity.

In order to display the asymmetry in the Kondo cloud more visibly, we calculate the ratio $S^x_{\mathbf{i}}/S^z_{\mathbf{i}}$. In Figs. 7(a) and 7(b), we show this ratio as influenced by λ and μ, respectively. In both cases, the difference between $S^x_{\mathbf{i}}$ and $S^z_{\mathbf{i}}$ is an oscillating

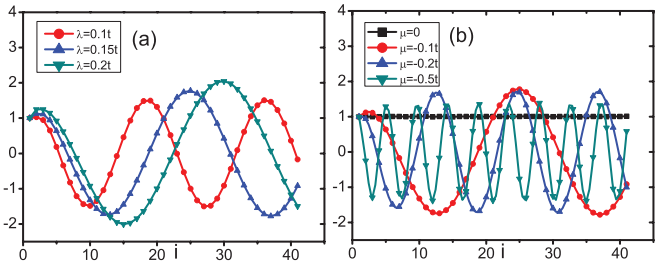

FIG. 7. (Color online) (a) The ratio $S^x_{\mathbf{i}}/S^z_{\mathbf{i}}$ with $\mu = -0.1t$. (b) The ratio $S^x_{\mathbf{i}}/S^z_{\mathbf{i}}$ with $\lambda = 0.15t$ varied. In both panels $U = 1.2t = -2\varepsilon_d$, and $\beta = 32t^{-1}$.

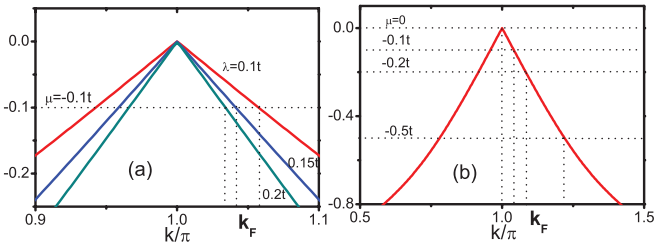

FIG. 8. (Color online) Schematics of extracting the Fermi vectors k_F from the band of $H_{\mathrm{K-M}}$. (a) μ is fixed at $-0.1t$ and $\lambda = 0.1t, 0.15t$, and $0.2t$. (b) λ is fixed at $0.15t$ and $\mu = 0, -0.1t, -0.2t$, and $-0.5t$. Solid lines represent the bands for the Kane-Mele Hamiltonian.

factor, whose maximum and minimum is a constant, so we can conclude that $S^z_{\mathbf{i}}$ and $S^x_{\mathbf{i}}$ have the same decay part, $f(R_{\mathbf{i}}) \propto g(R_{\mathbf{i}})$. For the wave vector ϕ of the oscillation part, Fig. 7 shows that ϕ increases both as λ and μ decreases. We recognize that these behaviors of ϕ have the similarity to that of the Fermi vector k_F, so in Fig. 8 we extract the k_F of $H_{\mathrm{K-M}}$ with the same values of λ and μ as in Fig. 7. Comparing ϕ to the Fermi vector k_F in Fig. 9, we see that the difference between ϕ and k_F is just a π, so ϕ and k_F can be regarded as the same. We can conclude that

$$S^z_{\mathbf{i}} \propto -\frac{-1}{f(R_{\mathbf{i}})}, \qquad S^x_{\mathbf{i}} \propto -\frac{-1}{f(R_{\mathbf{i}})}\cos 2k_F R_{\mathbf{i}}. \tag{7}$$

In Fig. (10), we study the effects of U on the ratio $S^x_{\mathbf{i}}/S^z_{\mathbf{i}}$. It is shown that the amplitude of oscillation can be enhanced, but the wave vector does not change as U increases.

From Figs. 6–10, we numerically study $S^x_{\mathbf{i}}$ and $S^z_{\mathbf{i}}$ in detail. The anisotropy in the Kondo cloud described by these correlators is originated from the fact that the transverse correlation function $S^x_{\mathbf{i}}$ has a spin-flip process and involves the contribution from the Kramers pair $(k\sigma, -k\bar{\sigma})$; hence display $2k_F$ oscillations on the Fermi level. While in the vertical one $S^z_{\mathbf{i}}$, there is only forward scattering within the left or right movers, which have fixed spin orientation, so it has no oscillations. This is purely due to the helical properties at the edge, and based on this point, we also find that the charge-charge correlation $N_{\mathbf{i}} = \langle (d^\dagger_\uparrow d_\uparrow + d^\dagger_\downarrow d_\downarrow)(c^\dagger_{\mathbf{i}\uparrow} c_{\mathbf{i}\uparrow} + c^\dagger_{\mathbf{i}\downarrow} c_{\mathbf{i}\downarrow})\rangle$ is similar to $S^z_{\mathbf{i}}$. Additionally, if we calculate the correlation functions between the impurity and B-sublattice sites at the

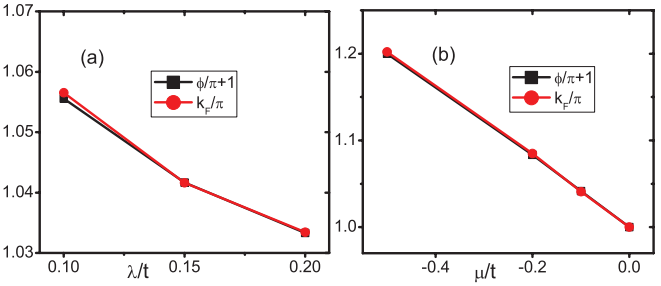

FIG. 9. (Color online) Comparing ϕ to the Fermi vectors k_F. (a) is for Figs. 7(a) and 8(a) and (b) is for Figs. 7(b) and 8(b).

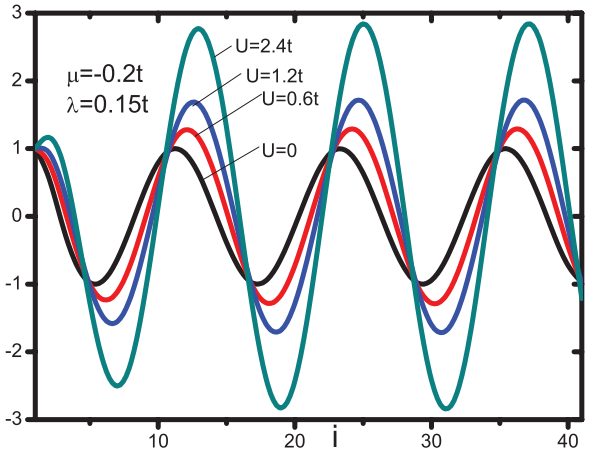

FIG. 10. (Color online) The ratio $S^x_{\mathbf{i}}/S^z_{\mathbf{i}}$ in the case of $\mu = -0.2t$ and $\lambda = 0.15t$ with U varied. $\beta = 32t^{-1}$ and ε_d is fixed at $-U/2$.

edge, they have the same behavior as Eq. (7). Finally, as for the decay function $f(R_{\mathbf{i}})$, here we cannot capture its exact formula in our simulation. While in Ref. 16, about an Anderson impurity coupled to a one-dimensional wire, the function $f(R_{\mathbf{i}})$ has the asymptotic behavior as $R^2_{\mathbf{i}}$.

From the QMC results for a magnetic impurity in the Kane-Mele model, it is shown that the LDOS is greatly modified by the SOC; thus the local properties of the local moment are mainly controlled by the LDOS of edge states, but these local quantities cannot show the topological phase in the system. In correlation functions linking electrons of the impurity and conducting bands, the interplay of the spin flip and backscattering is clearly seen; at the same time, due the SOC, the symmetry of spin rotation in the Kondo cloud is partly broken. So the topological phase transition is significantly reflected in these nonlocal physical quantities.

V. DISCUSSION AND CONCLUSION

In this paper, we study an Anderson impurity on a zigzag graphene ribbon undergoing a topological phase transition driven by a Kane-Mele type SOC. Using QMC simulations, we investigate both the local and nonlocal properties of the impurity. We find that with the SOC increasing from zero, the formation of a local moment is supported and the impurity behavior crosses over from a spin in a band with zero width to one in a normal metal. This is because the SOC decreases the LDOS at the edge and weakens the coupling between the impurity and conducting electrons. As for nonlocal properties, we clearly see the helical locking and the collaboration of backscattering and spin flip in the two-particle correlators and find a broken spin rotation symmetry in spin-spin correlation functions.

Although the intrinsic SOC of carbon atoms is weak,[17] a strong SOC can be achieved by heavy-atom doping[18–23] and tuned by a gate bias.[24] The magnetic impurity could be naturally realized by dangling σ bonds in graphene.[25] And recent developments in the field of spin-polarized scanning tunneling microscope[26] open the possibility to detect the Kondo cloud around the impurity (spin-spin correlations).

ACKNOWLEDGMENTS

This work was supported by the Academy of Finland through its Center of Excellence (2012-2017) program. The work of J.E.G. was supported by the US Department of Energy. We acknowledge computational resources from the CSC-IT Center for Science Ltd. and the Aalto local cluster Triton.

[1] Xiao-Liang Qi and Shou-Cheng Zhang, Rev. Mod. Phys. **83**, 1057 (2011).
[2] C. Wu, B. A. Bernevig, and S. C. Zhang, Phys. Rev. Lett. **96**, 106401 (2006).
[3] C. Xu and J. E. Moore, Phys. Rev. B **73**, 045322 (2006).
[4] Joseph Maciejko, Chaoxing Liu, Yuval Oreg, Xiao-Liang Qi, Congjun Wu, and Shou-Cheng Zhang, Phys. Rev. Lett. **102**, 256803 (2009).
[5] Yoichi Tanaka, A. Furusaki, and K. A. Matveev, Phys. Rev. Lett. **106**, 236402 (2011).
[6] Xiao-Yong Feng, Wei-Qiang Chen, Jin-Hua Gao, Qiang-Hua Wang, and Fu-Chun Zhang, Phys. Rev. B **81**, 235411 (2010).
[7] L. Isaev, D. F. Agterberg, and I. Vekhter, Phys. Rev. B **85**, 081107 (2012).
[8] Rok Žitko and Janez Bonča, Phys. Rev. B **84**, 193411 (2011).
[9] Mahdi Zarea, Sergio E. Ulloa, and Nancy Sandler, Phys. Rev. Lett. **108**, 046601 (2012).
[10] Katsunori Wakabayashi, Mitsutaka Fujita, Hiroshi Ajiki, and Manfred Sigrist, Phys. Rev. B **59**, 8271 (1999).
[11] C. L. Kane and E. J. Mele, Phys. Rev. Lett. **95**, 226801 (2005).
[12] J. E. Hirsch and R. M. Fye, Phys. Rev. Lett. **56**, 2521 (1986).
[13] J. E. Gubernatis, J. E. Hirsch, and D. J. Scalapino, Phys. Rev. B **35**, 8478 (1987).
[14] A. C. Hewson, *The Kondo Problem to Heavy Fermions* (Cambridge University Press, Cambridge, 1993).
[15] F. M. Hu, J. E. Gubernatis, Hai-Qing Lin, Yan-Chao Li, and R. M. Nieminen, Phys. Rev. B **85**, 115442 (2012).
[16] L. Borda, Phys. Rev. B **75**, 041307 (2007).
[17] Daniel Huertas-Hernando, F. Guinea, and Arne Brataas, Phys. Rev. B **74**, 155426 (2006).
[18] A. H. Castro Neto and F. Guinea, Phys. Rev. Lett. **103**, 026804 (2009).
[19] Samir Abdelouahed, A. Ernst, J. Henk, I. V. Maznichenko, and I. Mertig, Phys. Rev. B **82**, 125424 (2010).
[20] Zhenhua Qiao, Shengyuan A. Yang, Wanxiang Feng, Wang-Kong Tse, Jun Ding, Yugui Yao, Jian Wang, and Qian Niu, Phys. Rev. B **82**, 161414(R) (2010).
[21] Conan Weeks, Jun Hu, Jason Alicea, Marcel Franz, and Ruqian Wu, Phys. Rev. X **1**, 021001 (2011).
[22] Jun Ding, Zhenhua Qiao, Wanxiang Feng, Yugui Yao, and Qian Niu, Phys. Rev. B **84**, 195444 (2011).
[23] J. Chae, S. Jung, A. F. Young, C. R. Dean, L. Wang, Y. Gao, K. Watanabe, T. Taniguchi, J. Hone, K. L. Shepard, P. Kim, N. B. Zhitenev, and J. A. Stroscio, Phys. Rev. Lett. **109**, 116802 (2012).
[24] Zhuoyu Chen, Hongtao Yuan, Yanfeng Zhang, Kentaro Nomura, Teng Gao, Yabo Gao, Hidekazu Shimotani, Zhongfan Liu, and Yoshihiro Iwasa, Nano Lett. **12**, 2212 (2012).
[25] M. A. Cazalilla, A. Iucci, F. Guinea, and A. H. Castro Neto, arXiv:1207.3135.
[26] Lihui Zhou, Jens Wiebe, Samir Lounis, Elena Vedmedenko, Focko Meier, Stefan Blügel, Peter H. Dederichs, and Roland Wiesendanger, Nat. Phys. **6**, 187 (2010).